*Inorg. Chem.* **2003**, *42*, 1908–1918


# Electronic Structure of $ReO_3Me$ by Variable Photon Energy Photoelectron Spectroscopy, Absorption Spectroscopy and Density Functional Calculations

**Monica de Simone,[†] Marcello Coreno,[‡] Jennifer C. Green,*[,§] Sean McGrady,[||] and Helen Pritchard[||]**

*Dipartimento di Fisica "E. Amaldi", Università di Roma Tre ed Unità INFM, Roma, Italy, IMIP-CNR, Montelibretti, Italy, Unità INFM-TASC, Trieste, Italy, Inorganic Chemistry Laboratory, University of Oxford, South Parks Road, Oxford OX1 3QR, U.K., and Chemistry Department, Kings College, The Strand, London WC2R 2LS, U.K.*

Received September 10, 2002

Valence photoelectron (PE) spectra have been measured for $ReO_3Me$ using a synchrotron source for photon energies ranging between 20 and 110 eV. Derived branching ratios (BR) and relative partial photoionization cross sections (RPPICS) are interpreted in the context of a bonding model calculated using density functional theory (DFT). Agreement between calculated and observed ionization energies (IE) is excellent. The 5d character of the orbitals correlates with the 5p → 5d resonances of the associated RPPICS; these resonances commence around 47 eV. Bands with 5d character also show a RPPICS maximum at 35 eV. The RPPICS associated with the totally symmetric $4a_1$ orbital, which has s-like character, shows an additional shape resonance with an onset of 43 eV. The PE spectrum of the inner valence and core region measured with photon energies of 108 and 210 eV shows ionization associated with C 2s, O 2s, and Re 4f and 5p electrons. Absorption spectra measured in the region of the O1s edge showed structure assignable to excitation to the low lying empty "d" orbitals of this $d^0$ molecule. The separation of the absorption bands corresponded with the calculated orbital splitting and their intensity with the calculated O 2p character. Broad bands associated with Re 4d absorption were assigned to $^2D_{5/2}$ and $^2D_{3/2}$ hole states. Structure was observed associated with the C1s edge but instrumental factors prevented firm assignment. At the Re 5p edge, structure was observed on the $^2P_{3/2}$ absorption band resulting from excitation to the empty "d" levels. The intensity ratios differed from that of the O 1s edge structure but were in good agreement with the calculated 5d character of these orbitals. An absorption was observed at 45 eV, which, in the light of the resonance in the $4a_1$ RPPICS, is assigned to a $4a_1 \rightarrow ne$, $na_2$ transition. The electronic structure established for $ReO_3Me$ differs substantially from that of $TiCl_3Me$ and accounts for the difference in chemical behavior found for the two complexes.

## Introduction

Variable photon energy photoelectron spectroscopy (PES) provides a powerful method of probing the electronic structure of molecules.[1] In particular, the very different partial cross section behavior of d and f electrons compared with that of s and p electrons provides extensive information on metal−ligand covalency. Electrons with high angular momentum are not only distinguished in their one-electron cross sections, which have maxima some way from the threshold but undergo strong resonances. In the case of d electrons, these are a consequence of resonant absorption from the core $(n - 1)$ p shell to the valence $(n - 1)$ d shell followed by super Coster Kronig (SCK) decay, which results in repopulation of the p hole, and ejection of an electron with d character. Thus, the final state has identical energy to that from direct photoionization. Opening this second channel at photon energies close to the absorption energy gives additional features in the photoionization cross section char-

* To whom correspondence should be addressed. E-mail: jennifer.green@chemistry.oxford.ac.uk.
[†] Università di Roma Tre ed Unità INFM.
[‡] IMIP-CNR and Unità INFM-TASC.
[§] University of Oxford.
[||] Kings College.

(1) Green, J. C. *Acc. Chem. Res.* **1994**, *27*, 131.



10.1021/ic020547+ CCC: $25.00 
Published on Web 02/21/2003

acterized by Fano profiles. It is also possible to detect the resonance processes that cause the additional channel by absorption spectroscopy.

Observation of such giant resonances in a PE cross section not only leads to firm identification of d and f bands but also gives evidence of metal ligand d or f covalency when they arise in what is primarily a ligand PE band.

Such studies of classic tetrahedral molecules such as $TiCl_4$[2] and $OsO_4$[1] have produced unambiguous assignments of the PE bands; in the case of $OsO_4$, the assignment was new and gave evidence of interaction of the 5p core with the valence electrons.[3] These pseudoisoelectronic molecules have very different orbital energy sequences which can be related to the dominance of the nature of the contributing metal orbital in the Os case. Related studies on $TiCl_3Me$,[4] free of $TiCl_4$ contaminant, enabled identification of all the valence orbitals. In this case, the highest occupied molecular orbital (HOMO) was found to be a localized Ti−C bond. Here, we extend this series to $ReO_3Me$.

The electronic structure of $ReO_3Me$ and the nature of the Re−C and Re═O moieties is of particular interest in light of its remarkably wide activity as an organometallic catalyst, with particular utility in the areas of oxidation and olefin metathesis.[5] In addition, $ReO_3Me$ provides a comparison with the isoelectronic $T_d$ species $OsO_4$, as well as affords an isostructural but chemically very different comparison with the $C_{3v}$ molecule $TiCl_3Me$.

## Experimental Section

$ReO_3Me$ was prepared by a literature method involving the interaction of $Re_2O_7$ with $SnMe_4$ in THF solution.[6] The product was purified by repeated sublimation in vacuo, and its purity was assessed by reference to its $^1H$ NMR and IR spectra.[7]

The PE spectral measurements were carried out on the undulator based gas-phase photoemission beamline at ELETTRA, Trieste,[8] using the angle resolved photoelectron spectrometer (ARPES) chamber and an ionization cell.[9] The monochromator is a VASGM (variable angle spherical grating monochromator), working with four gratings to cover the energy 15−1000 eV, with a mean energy resolution $\Delta E/E \geq 10.000$. Photoelectron spectra could be normalized using the signal from a calibrated photodiode (IRD, Inc.), while absorption spectra were normalized to the signal due to the incoming photon flux detected by a gold mesh.

A sample of $ReO_3Me$, contained in a glass ampule wrapped in aluminum foil, was held under vacuum in a thermal bath at room temperature external to the spectrometer. Its vapor was introduced via a 6 mm tube open near the ionization region.

The ARPES chamber was equipped with a 50 mm mean radius electron energy analyzer (VSW Ltd.), mounted at the magic angle. A pass energy of 10 eV, corresponding to a resolution of 200 meV, was used for valence states photoelectron spectra (PES). Core and inner valence spectra were recorded using a pass energy of 25 eV, corresponding to a resolution of 0.5 eV. The overall gas pressure was held at about $4 \times 10^{-6}$ mbar.

PE spectra of the valence region, binding energy 10.5−17 eV, were measured at the magic angle for a series of photon energies ranging from 23 to 67 eV, using a grating with 400 l/mm, and 67−110 eV, using a grating with 1200 l/mm. Normally three to four spectra were measured at each photon energy. Photoelectron spectra of He were measured over the same ranges for intensity calibration purposes. Photon energy bandwith $\Delta E$ was better than 30 meV for photon energies below 110.5 eV, so the total energy bandwidth for PE spectra is mainly due to the photoelectron analyzer.

Core and inner valence spectra were measured using a 150 mm VG photoelectron analyzer, using photon energies of 108, 210, and 330 eV.

Re 4f/5d edge region absorption spectra were measured over the photon energy range 35−85 eV using a grating with 400 l/mm, with a photon energy bandwidth varying from 3 to 10 meV. The acquisition in this photon energy range was possible through the parallel scan of the undulator GAP and of the dispersed wavelength from VASGM. Normalization of data, using the electron yield from a gold mesh before the interaction region, gave, as a result, a complete removal of the wiggles due to the sawtooth shape of $I_0$.

X-ray absorption spectra at the Re 4d, C 1s, and O 1s edges were acquired with gratings with 1200 l/mm and a photon energy resolution better than 100 meV. Unfortunately, there is a strong decrease of photon flux in the region of the carbon 1s edge due to adsorbed carbon on the first optical elements of the beamline. As a consequence, the absorption spectrum in the region 290−300 eV is not relaible. The O 1s spectrum was acquired by operating the undulator in the wiggler mode (GAP = 30.1 mm).

To obtain branching ratios (BR) and cross sections (CS) for the various valence bands, the data points were divided by the beam intensity measured during the course of a run by a calibrated photodiode positioned after the ionization region in the path of the beam. The normalized spectra at each photon energy were compared to verify consistency and converted into a time weighted average spectrum. Spectra were then fitted with Gaussian peaks using the routine available in IGOR Pro with background subtraction. An example of this fitting procedure is given in Figure 1. Branching ratios were available directly from the areas of the Gaussians. Relative partial photoionization cross sections (RPPICS) were obtained using the He calibration data. Comparison of the measured intensities ($I_{exp}$) with the absolute cross sections ($I_{abs}$) showed a fairly consistent ratio for each grating except at the extremities of the grating ranges. The measured band intensities were multiplied by the ratio $I_{abs}/I_{exp}$ to correct for instrumental bias.

Density functional calculations were performed using the Amsterdam Density Functional code (version ADF2000.02).[10] Scalar relativistic corrections were included via the ZORA method.[11,12]

(2) Bursten, B. E.; Green, J. C.; Kaltsoyannis, N.; MacDonald, M. A.; Sze, K. H.; Tse, J. S. *Inorg. Chem.* **1994**, *33*, 5086.
(3) Bursten, B. E.; Green, J. C.; Kaltsoyannis, N. *Inorg. Chem.* **1994**, *33*, 2315.
(4) Field, C. N.; Green, J. C.; Kaltsoyannis, N.; McGrady, G. S.; Moody, A. N.; Siggel, M.; De Simone, M. *J. Chem. Soc., Dalton Trans.* **1997**, 213.
(5) Romão, C. C.; Kühn, F. E.; Herrmann, W. A. *Chem. Rev.* **1997**, *97*, 3197.
(6) Herrmann, W. A.; Kiprof, P.; Rypdal, K.; Tremmel, J.; Blom, R.; Alberto, R.; Behm, J.; Albach, R. W.; Bock, H.; Solouki, B.; Mink, J.; Lichtenberger, D.; Gruhn, N. E. *J. Am. Chem. Soc.* **1991**, *113*, 6527.
(7) Herrmann, W. A.; Kuchler, J. G.; Felixberger, J. K.; Herdtweck, E.; Wagner, W. *Angew. Chem., Int. Ed. Engl.* **1988**, *27*, 394.
(8) Prince, K. C.; Blyth, R. R.; Delaunay, R.; Zitnik, M.; Krempasky, J.; Slezak, J.; Camilloni, R.; Avaldi, L.; Coreno, M.; Stefani, G.; Furlani, C.; de Simone, M.; Stranges, S. *J. Synchrotron Radiat.* **1998**, *5*, 565.
(9) Fronzoni, G.; de Simone, M.; Coreno, M.; Prince, K. C.; Furlan, S.; Franceschi, P.; Decleva, P. *J. Phys. Chem.*, submitted.
(10) Baerends, E. J. *ADF2000.02*; Department of Theoretical Chemistry, Vrije Universiteit: Amsterdam, 2000.
(11) van Lenthe, E.; van Leeuwen, R.; Baerends, E. J.; Snijders, J. G. *Int. J. Quantum Chem.* **1996**, *57*, 281.
(12) van Lenthe, E.; Snijders, J. G.; Baerends, E. J. *J. Chem. Phys.* **1996**, *105*, 6505.

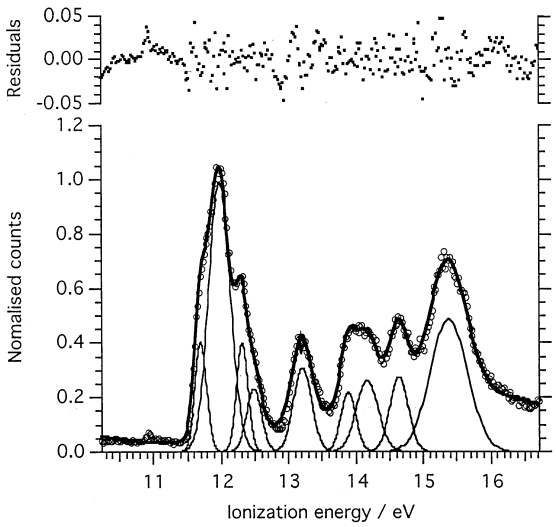


**Figure 1.** Typical fit of the valence region of the PE spectrum of $ReO_3$-Me with Gaussian functions.

The generalized gradient approximation was employed, using the local density approximation of Vosko, Wilk, and Nusair[13] together with nonlocal exchange correction by Becke[14] and nonlocal correlation corrections by Perdew.[15] Type IV basis sets were used with triple $\zeta$ accuracy sets of Slater type orbitals, with a single polarization function added to the main group atoms. The cores of the atoms were frozen up to 1s for C and O, and 4d for Re. Ionization energies were calculated by direct calculations on the molecular ions in their ground and appropriate excited states, and subtraction of the energy of the neutral molecule. Spin−orbit calculations, as available in the ADF program suite, were also carried out both on the ground state molecule and the molecular ion states.

## Results

Valence photoelectron spectra of $ReO_3Me$ measured at four different photon energies are shown in Figure 2. Ionization energies of the principal features are given in Table 1 and are in agreement with the literature data.[6,16] Band C shows two features on the high energy edge consistent with a vibrational progression of $1411 \pm 80$ cm$^{-1}$. The closest totally symmetric mode in the vibrational spectrum of the molecule is at 1210.4 cm$^{-1}$ and is assigned to a $\delta_s(CH_3)$ mode.[17]

Branching ratios (BR) for bands A−G are shown in Figure 3. Because of the difficulty of deconvoluting bands A, B, and C over the whole energy range, their combined intensity was used to generate the BR. (The relative intensities of A, B, and C are discussed in a following paragraph.)

Using the He calibration data, relative partial cross sections were generated and are shown in Figure 4. Though the He calibration corrected well for the grating change, there is a small discontinuity in all the curves at 67 eV which coincides with the grating change. No such discontinuity is found in the BR data.

Inner valence and core PE spectra were measured with photon energies of 79.5 and 110.5 eV. $N_2$ was used to

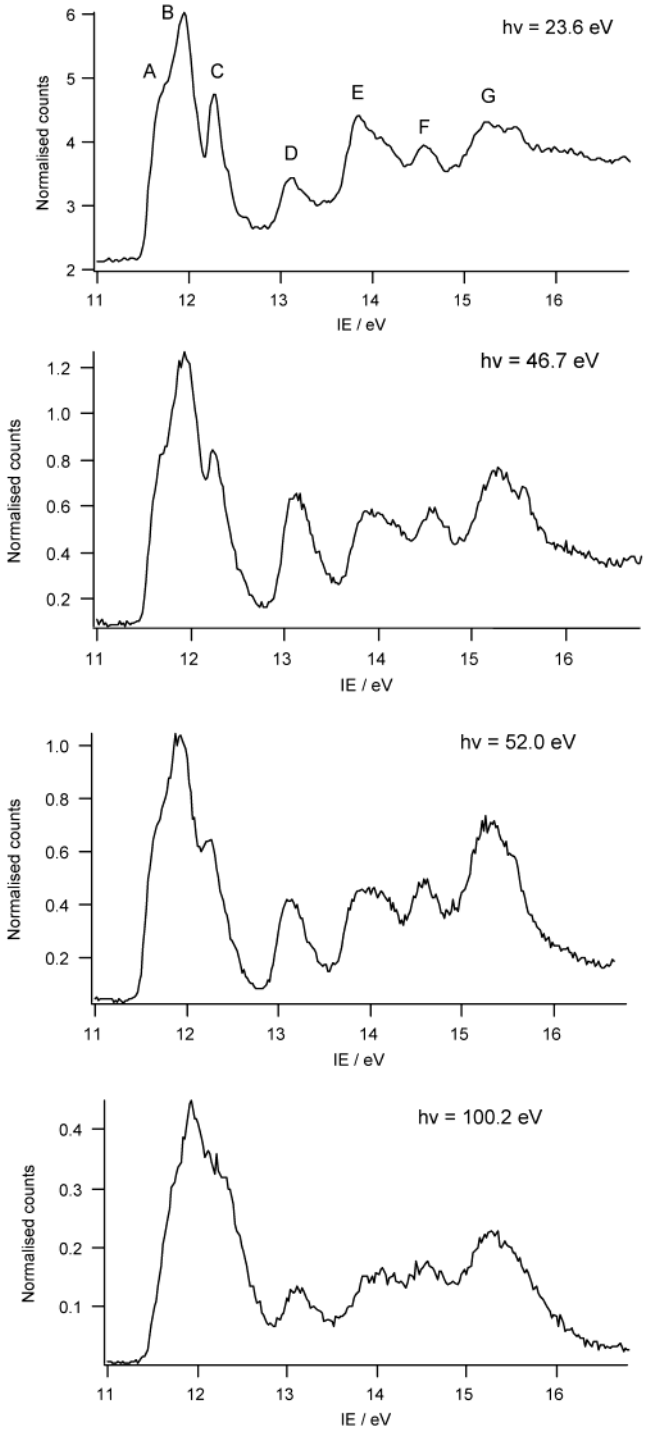


**Figure 2.** PE spectrum of $ReO_3Me$ measured with photon energies of 23.6, 46.7, 52.0, and 100.2 eV.

**Table 1.** Vertical Ionization Energies (eV) for $ReO_3Me$

| | band | | | | | | |
|---|---|---|---|---|---|---|---|
| | A | B | C | D | E | F | G |
| IE | 11.63 | 11.94 | 12.27<br>(12.44)<br>(12.62) | 13.08 | 13.83<br>14.08 | 14.54 | 15.26 |

(13) Vosko, S. H.; Wilk, L.; Nusair, M. *Can. J. Phys* **1990**, *58*, 1200.
(14) Becke, A. D. *Phys. Rev.* **1988**, *A38*, 2398.
(15) Perdew, J. *Phys. Rev.* **1986**, *B33*, 8822.
(16) Köstlmeier, S.; Häberlen, O. D.; Rösch, N.; Herrmann, W. A.; Solouki, B.; Bock, H. *Organometallics* **1996**, *15*, 1872.
(17) Morris, L. J.; Downs, A. J.; Greene, T. M.; McGrady, G. S.; Herrmann, W. A.; Sirsch, P.; Scherer, W.; Gropen, O. *Organometallics* **2001**, *20*, 2344.

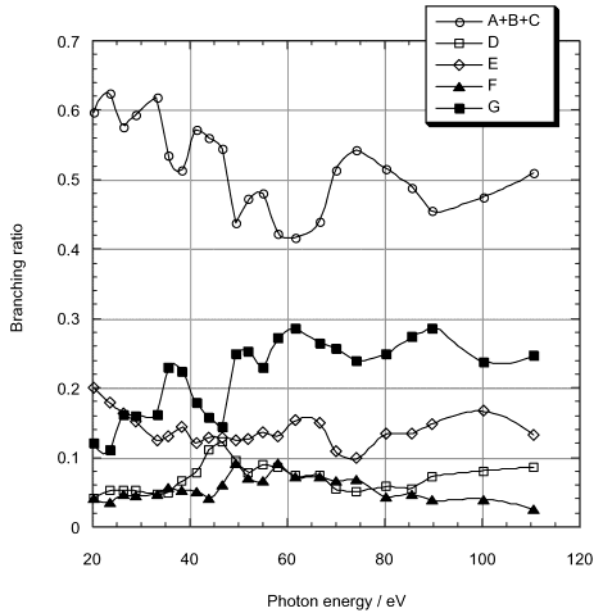


**Figure 3.** Branching ratios for the valence bands of $ReO_3Me$.

**Table 2.** Calculated and Experimental Bond Lengths (Å) and Angles (deg) for $ReO_3Me$

| | Re−C | Re−O | C−H | O−Re−C | H−C−Re |
|---|---|---|---|---|---|
| calcd | 2.090 | 1.723 | 1.098 | 106.3 | 108.9 |
| exptl | 2.060(9) | 1.709(3) | 1.105(1.2) | 106.0 | 112(3) |

calibrate the inner valence spectra. The C(1s) spectrum was calibrated assuming a 4 eV work function for the spectrometer.

Absorption spectra were measured in three regions, those of the O 1s edge (525−580 eV), the Re 4d and C 1s edges (250−305 eV), and the Re 4f and Re 5p edges (30−80 eV).

Density functional calculations were used to optimize the geometry of the molecule, with the constraint of $C_{3v}$ symmetry, in both eclipsed and staggered conformations. The energy of the staggered form was found to be lower by 7 kJ $mol^{-1}$. A frequency calculation confirmed this structure as a minimum on the energy surface. The bond lengths and angles calculated are compared in Table 2 with the experimental data.[6] Ionization energies for the valence, inner valence, and selected core orbitals were calculated. The ionization energies and the AO character of the valence orbitals (Table 3) are in good agreement with the results reported by Rösch and co-workers.[16] Calculations including spin−orbit coupling were also carried out using the optimized geometry obtained in its absence. Significant differences in ionization energy were only found for the 4f and 5d core orbitals.

## Discussion

$ReO_3Me$ has $C_{3v}$ geometry and a staggered conformation. Its MO structure may be viewed as a perturbation of a tetrahedral parent. Such an approach emphasizes the fact that most of the orbitals are delocalized over the whole molecule and cannot be associated primarily with either the O or the Me groups. Correlation of the orbitals with those of a $MO_4$ tetrahedron is shown in Figure 5, together with an isosurface

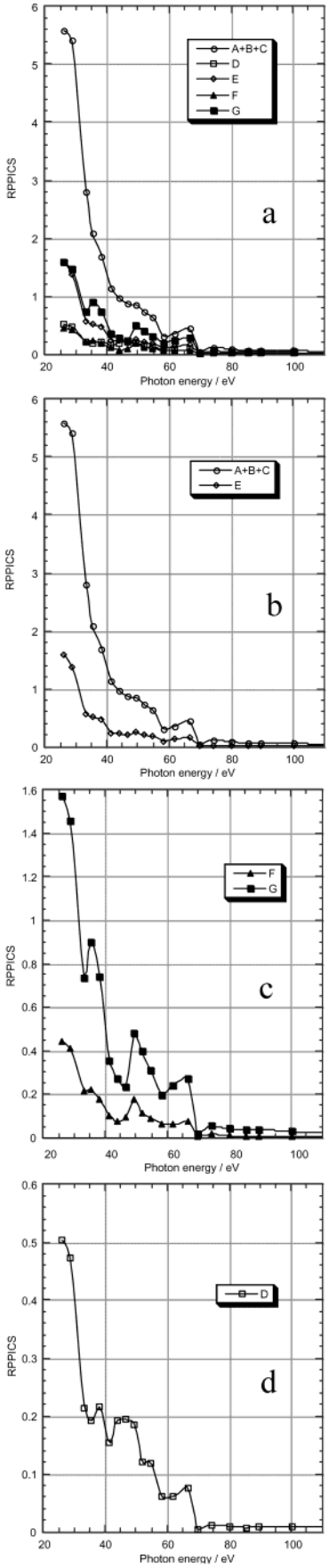


**Figure 4.** Relative partial photoionization cross sections for the valence bands of $ReO_3Me$: (a) all bands, (b) A + B + C and E, (c) F and G, (d) D.

**Table 3.** Band Assignment, Valence Orbital Energies (eV), Composition, and Calculated and Experimental IE (eV)

| band | assignment | orbital energy | orbital composition (%) Re | O 2p | C 2p | H 1s | calcd IE this work | calcd IE ref 16 | exptl IE |
|---|---|---|---|---|---|---|---|---|---|
| | 7e | −1.42 | 47 ($xz$, $yz$) 3 ($xy$, $x^2 - y^2$) | 42 | | | | | |
| | $6a_1$ | −2.15 | 43 ($z^2$) 5 ($z$) | 21 | 25 | | | | |
| | 6e | −4.11 | 45 ($xy$, $x^2 - y^2$) 10 ($x$,$y$) | 40 | | | | | |
| A | $1a_2$ | −8.11 | | 100 | | | 11.61 | 11.62 | 11.63 |
| B | 5e | −8.50 | | 96 | | | 11.88 | 11.93 | 11.94 |
| C | $5a_1$ | −8.82 | 7 ($z$) | 60 | 22 | | 11.96 | 11.96 | 12.27 |
| D | $4a_1$ | −9.95 | 8 (s) 6 ($z^2$) | 53 | 20 | | 13.14 | 13.28 | 13.08 |
| E | 4e | −10.40 | 16 ($xz$,$yz$) | 42 | 17 | 19 | 13.61 | 13.36 | 13.83 |
| F | $3a_1$ | −11.08 | 35 ($z^2$) | 50 | 6 | | 14.44 | 14.66 | 14.54 |
| G | 3e | −11.64 | 32 ($xy$, $x^2 - y^2$) 6 ($xz$,$yz$) | 51 | | | 14.93 | 14.95 | 15.26 |
| | 2e | −11.80 | 19 ($xz$,$yz$) 4 ($xy$, $x^2 - y^2$) | 19 | 26 | 23 | 15.43 | 15.39 | |

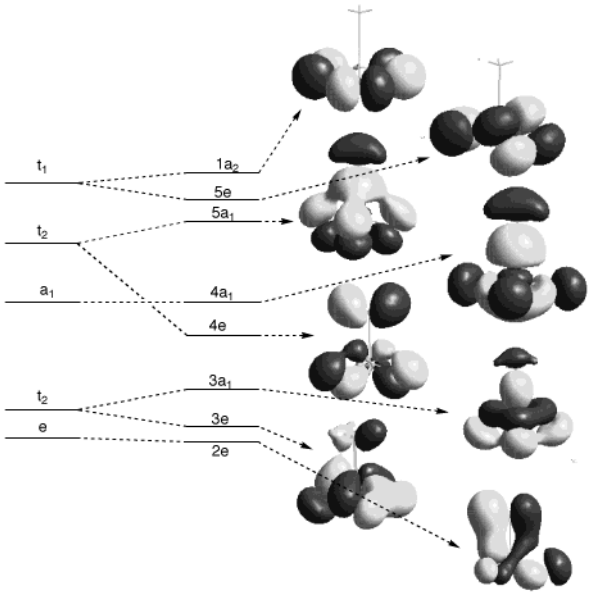


**Figure 5.** MO diagram and isosurfaces for the valence orbitals of $ReO_3$-Me. Correlation of the orbitals with those of a tetrahedral $MO_4$ unit is also shown.

for each energy level. The ordering for the $MO_4$ tetrahedron is taken from that established for $OsO_4$.[18] For these late third row transition metals, the metal AO contribution dominates the nodal properties of the MO and their energy ordering in that

$$e(5d) \sim t_2(5d) < a_1(6s) < t_2(6p) < t_1 \text{ (nonbonding)}$$

Replacement of O by $CH_3$ results in a major perturbation of the e levels as the $CH_3$ e orbitals are C−H bonding and considerably more stable than the O 2p$\pi$ levels.

The $1a_2$ and 5e orbitals are nonbonding and composed of O p$\pi$ orbitals. The $5a_1$ orbital shows a small Re 6p contribution and mixed $\sigma\,\pi$ characteristics for the ligand set, whereas the $4a_1$ orbital is ligand p$\sigma$ in character, but in this case mixed with Re 6s and 5d($z^2$). The 4e orbitals have small Re 5d contributions and significant C−H bonding character; the nodal surfaces shows the 4e level to be Re−C antibonding. Metal d character is at a maximum in the $3a_1$, 3e and 2e orbitals, the most tightly bound of the valence orbitals. The 2e pair are Re−C $\pi$ bonding.

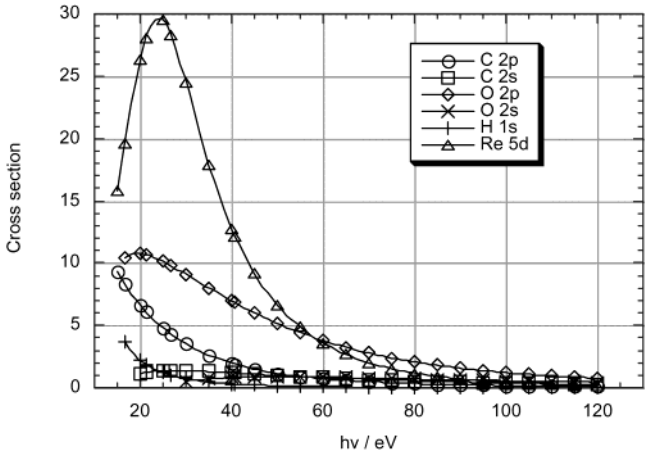


**Figure 6.** Calculated AO cross sections of O 2p, C 2p, H 1s, and Re 5d and 6s AO.

**RPPICS.** The RPPICS are most lucidly discussed in the context of the LCAO MO model already presented and the expected profiles of the AO cross sections.[19] Those calculated for one-electron cross sections of the relevant AO are shown in Figure 6. Though the magnitude of the AO cross sections is not exact, the general features and relative trends are well established. In addition, Re 5d bands are expected to show a giant resonance on excitation of the Re 5p subshell at approximately 45 and 56 eV. Such features have been observed in the branching ratios of the d bands of $Re(CO)_5X$, X = Cl, Br.[20] Comparison with RPPICS of analogous bands of $OsO_4$, $TiCl_4$, and $TiCl_3Me$ will also prove useful in assignment and identification of key features.

Figure 4a gives all RPPICS on the same plot. Figure 4b−d gives separate plots for those bands which show similar variations in cross section; the arbitrary vertical scale is constant in all plots.

**Bands F and G.** The branching ratios in Figure 3 show that bands F and G generally grow in relative intensity over the photon energy range 20−60 eV. Figure 4c shows a sharp intensity increase for these bands with an onset at 47 eV and a maximum at 50 eV. This is followed by a second less intense increase with an onset at 58 eV. (The grating change coincides with this resonance and makes the maximum difficult to define.) These features suggest a Re 5d contribu-

(18) Green, J. C.; Guest, M. F.; Hillier, I. H.; Jarrett-Sprague, S. A.; Kaltsoyannis, N.; MacDonald, M. A.; Sze, K. H. *Inorg. Chem.* **1992**, *31*, 1588.

(19) Yeh, J.-J. *Atomic calculation of photoionization cross-sections and asymmetry parameters*; Gordon and Breach Science Publishers: Langhorne, PA, 1993.

(20) Hu, Y. F.; Bancroft, M.; Tan, K. H. *Inorg. Chem.* **2000**, *39*, 1255.

tion to the MOs from which these bands originate. The features with an onset of 47 and 58 eV result from 5p−5d excitation and super Coster Kronig decay giving an additional channel for ionization of electrons with 5d character. There also is a peak with a maximum at 35 eV which may be a shape resonance, the excited state being an f wave trapped within the molecular potential. Alternatively, it could be associated with the delayed maximum in the 5d cross section (Figure 6) which is calculated to occur at a photon energy of 25 eV. The intensity ratio of band F to band G is approximately 1:4 over the whole photon energy range suggesting similar AO character and a degeneracy consistent with the assignment of band F to ionization of an $a_1$ orbital and G to two e orbitals. The DFT calculations (Table 3) confirm that the 2e, 3e, and $3a_1$ orbitals are those with the highest 5d character among the MOs, ranging from 23% to 38%.

These orbitals correlate with the 1e and $2t_2$ orbitals of $OsO_4$ which give rise to band 5 in its valence PE spectrum.[18] Giant resonances occur in the RPPICS of band 5 between 49 and 61 eV. They are somewhat stronger than those observed here for $ReO_3Me$, consistent with the higher d content which is calculated as 43% for $2t_2$ and 49% for 1e. The RPPICS of band 5 also shows maxima at low photon energies (27 and 36 eV).

**Band D.** Band D has a branching ratio consistent with the $4a_1$ ionization to which it is assigned. Its RPPICS (Figure 4d) has features in common with bands F and G, but there are also significant differences, which are emphasized by comparing the branching ratios of bands D and F; they are both associated with nondegenerate orbitals and thus have BR of comparable magnitude. A rise in cross section occurs at 43 eV, earlier than that found for bands F and G; consequently, the maximum between 40 and 50 eV is broader. This suggests that, in addition to a small p−d resonance, there is another resonance preceding it. A small maximum is also shown at 38 eV, slightly higher in energy than that observed in bands F and G. Again, excitation to a trapped f wave is implicated, but the different symmetry of the ground state orbital may account for the energy difference of the resonance. At high photon energies, band D gains in intensity relative to band F.

Calculation shows the associated $4a_1$ orbital to have a small admixture of both Re 5d and Re 6s character. It is more ligand localized than any of the orbitals giving rise to bands F and G. The related $OsO_4$ orbital, $2a_1$, has 17% Os 6s character and, by symmetry, no d contribution. The RPPICS of the associated $OsO_4$ PE band, band 4, shows a pronounced maximum at 48 eV; the RPPICS of the totally symmetric orbital of $TiCl_4$ shows a peak at 40 eV. Thus, it is likely that the 43 eV rise in RPICCS of band D is a shape resonance which reveals the totally symmetric parentage of the $4a_1$ orbital. The excited state would be a p wave ($a_2$ or e symmetry in a $C_{3v}$ point group.) The relative increase in intensity at high photon energies compared to band F is most plausibly associated with the lower d content of the $4a_1$ orbital. In the photon energy range 60−120 eV, the 5d cross section is calculated to decrease more rapidly than that of the O 2p orbital (Figure 6).

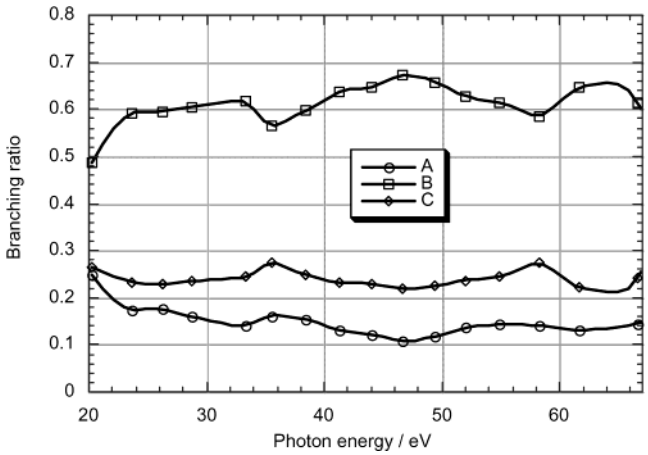


**Figure 7.** Branching ratios for bands A, B, and C in the photon energy region 23−67 eV.

**Bands A, B, C, and E.** The RPPICS of these bands show a general decrease with increasing photon energy with few irregularities consistent with their domination by the O 2p character of the associated orbitals. Band A, arising from the $1a_2$ orbital, is 100% O 2p character, and band B is calculated to be 96% O 2p. Both are related to the $1t_1$ orbital of $OsO_4$ to which band 1 is assigned. Band 1 also shows a relatively featureless decaying cross section. Band C has a different parentage; it is assigned to the $5a_1$ orbital which has mixed O 2p C 2s character. It is of interest to know whether band C has an RPPICS that can be differentiated from those of bands A and B. Separate fits to these three bands could be satisfactorily achieved for those spectra acquired with grating 1 and photon energies below 67 eV. The lower resolution with the higher grating led the deconvolution process to assign too great a proportion of the area to band C in our judgment. The branching ratios of bands A, B, and C are shown for the lower photon energy range in Figure 7. No really significant variations were found.

**Inner Valence and Core PE Spectra.** PE spectra acquired with photon energies of 108 and 210 eV are shown in Figure 8. Ionization energies and assignments are listed in Table 4. The calculated cross sections[19] for C2s, O 2s, and Re 4f, 5s, and 5p orbitals are given in Figure 9.

The most prominent feature in the core region is the spin−orbit split doublet resulting from ionization of the 4f orbitals occurring at 52.5 and 55.0 eV. Calculations on the 4f ionization cross section show a rising intensity from threshold to a maximum at a photon energy of 235 eV (Figure 9).

Literature values on Re core ionizations suggest that the $^2F_{7/2}$ and $^2P_{3/2}$ core hole states are coincident and that the $^2P_{1/2}$ state lies 11 eV higher in energy.[21] For a photon energy of 108 eV, a broad structure is distinguishable underlying the $^2F_{7/2}$ band; this is assigned to the $^2P_{3/2}$ ion state. An even broader structure is also apparent centered at 64 eV which is suitably placed for the $^2P_{1/2}$ state. With the higher photon energy of 210 eV, the 4f cross section is very much greater

(21) *Handbook of X-ray and ultraviolet photoelectron spectroscopy*; Briggs, D., Ed.; Heyden: London, 1977.

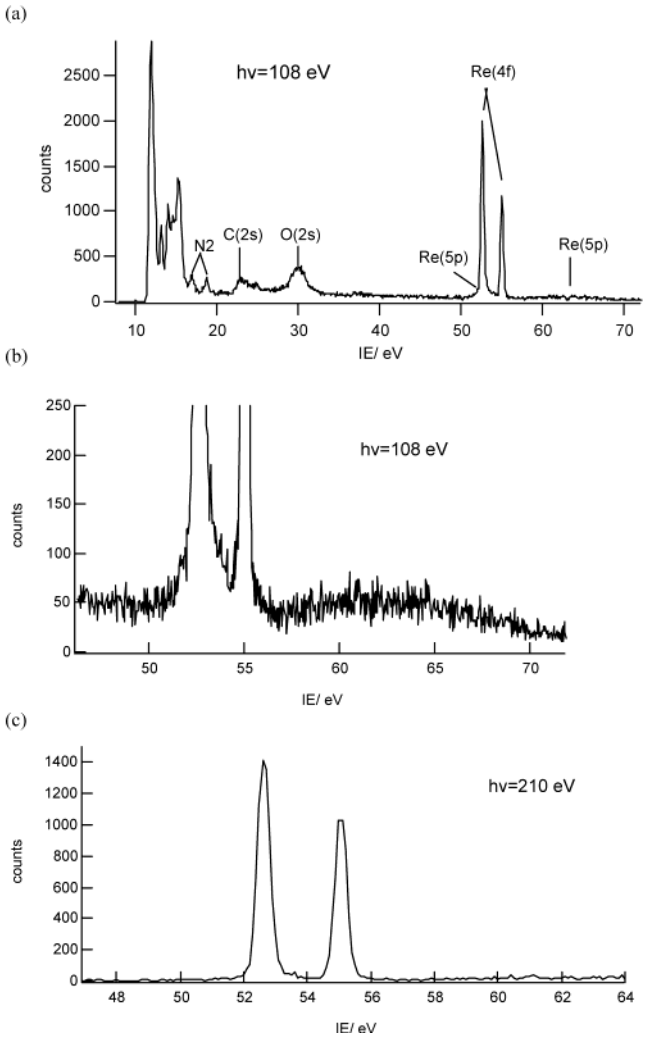


**Figure 8.** PE spectra of the valence, inner valence, and core region with photon energies of (a) 108 and (b) 210 eV.

**Table 4.** Core and Inner Valence Orbital Energies and Calculated and Experimental Ionization Energies (eV)

| atom | core orbital | orbital energy | IE calcd, no SO | core hole state | IE calcd, with SO | IE exptl | IE lit.[21] |
|---|---|---|---|---|---|---|---|
| Re | 5s | −87.67 | 92.62 | $^2S_{1/2}$ | 92.78 | | 86 |
| | 5p (*x*, *y*) | −50.15 | 54.74 | $^2P_{1/2}$ | 60.77 | 64 | 56 |
| | 5p (*z*) | −49.76 | 54.37 | $^2P_{3/2}$ | 56.75 | 53 | 45 |
| | 4f | −45.57 to −45.51 | 54.2 | $^2F_{5/2}$ | 53.22 | 55.0 | 47 |
| | | | | $^2F_{7/2}$ | 51.79 | 52.5 | 45 |
| O | 2s ($1a_1$) | −24.50 | 28.13 | | 28.24 | 29.8 | 28.48 |
| | 2s (1e) | −23.92 | 27.55 | | 27.51 | | |
| C | 2s ($2a_1$)[a] | −18.31 | 22.48 | | 22.72 | 22.9 | 16.59 |
| | 1s | | | $^2S_{1/2}$ | 291.4 | 286.5 | 288 |

[a] The $2a_1$ orbital has 57% C 2s and 39% H 1s character.

than that of 5p, making the 4f signal much cleaner and the 5p less visible.

The IE values for the f bands are considerably higher than those found for Re pentacarbonyl derivatives reported by Hu et al. which ranged from 47.5 to 48.3 and 49.9 to 50.7 eV.[20] The shift is undoubtedly accounted for by the electronegative O in $ReO_3Me$. With photon energies between 70 and 80 eV, the $^2P_{3/2}$ state was observed, intermediate between the two $^2F$ states, in the range 48.4−50 eV. The $^2P_{1/2}$ state was not detected.

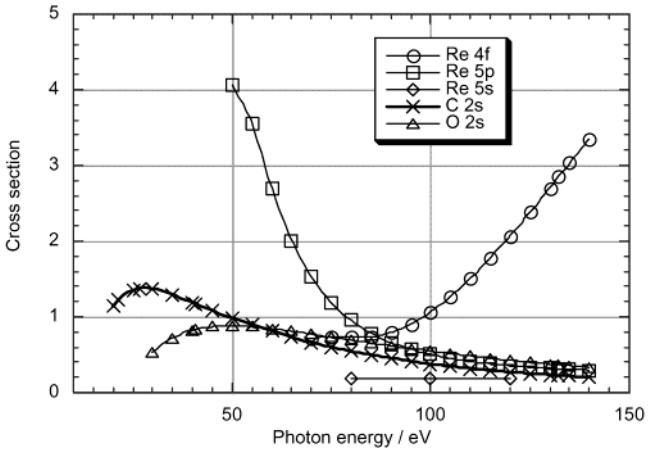


**Figure 9.** Calculated cross sections for Re 4f, Re 5p, Re 5s, C 2s, and O 2s ionizations.

Bands in the inner valence region at 22.9 and 29.8 eV may be associated with the C 2s and O 2s ionizations, respectively. They are broader than the f bands. The $2a_1$ orbital is C−H bonding with 57% C 2s character so the width in this case is likely to be caused in part by unresolved vibrational structure. Shake up structure is evident on the C(2s) band at 24.9 eV. Two orbital ionizations are associated with the O 2s band, $1a_1$ and 1e, which the calculations place 0.6 eV apart. These can both be accommodated within the observed bandwidth.

A C(1s) signal was observed at 286.5 eV using a photon energy of 330 eV (there was no internal calibrant for this band).

Inner valence and core ionizations were calculated in two ways, neglecting and including the effects of spin−orbit coupling. The resulting calculated IEs are given in Table 4.

For the O 2s and C 2s IEs, inclusion of spin−orbit SO coupling made little difference. The calculations are in good agreement with experiment for the $2a_1$ band, but for the O 2s band, the calculated IE was 1 eV too low.

The calculation omitting SO coupling gave an IE for the 4f band between the values for the two SO states found experimentally. The calculation with SO coupling gave lower values and a splitting of 1.4 eV whereas the experimental separation was 2.5 eV.

Neglect of spin−orbit coupling puts the Re 5p ionization coincident with the 4f. Inclusion of SO coupling gives significantly higher values for the 5p ionizations with an SO splitting of 4 eV. This is considerably less than the literature value of 11 eV.

Thus, the SO calculations for core ionizations tend to give somewhat less reliable values for the IE and underestimate the SO splittings.

**Absorption Spectra.** VUV and X-ray absorption spectra acquired with photon energies between 35 and 530 eV are shown in Figures 10−12. Excitation energies and assignments are listed in Table 5.

These experiments served two principal purposes. First, excitations from core 1s orbitals to unoccupied valence levels may be used to map the 2p content of the virtual orbitals. Thus, the near edge structure in the O 1s absorption spectrum

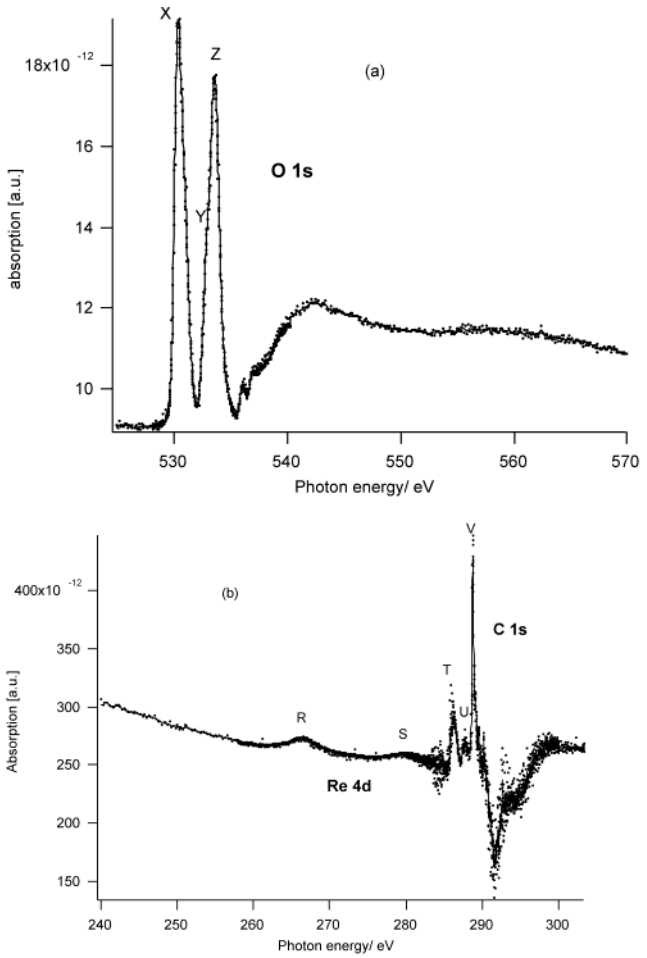


**Figure 10.** Absorption spectra of $ReO_3Me$ in the regions (a) 525−570 and (b) 250−305 eV.

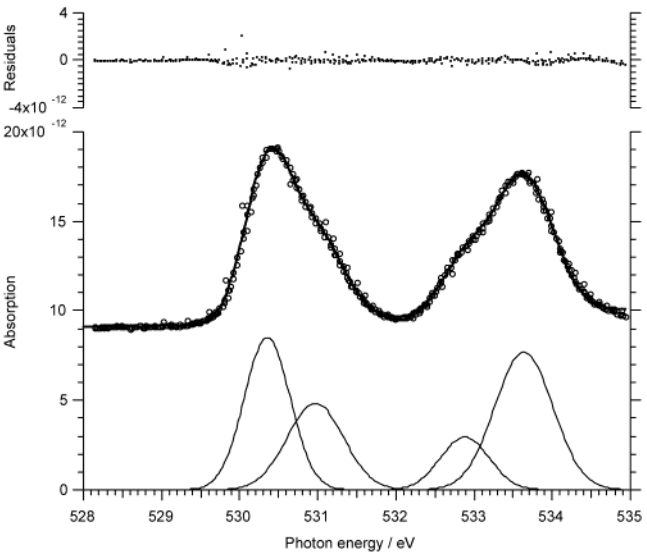


**Figure 11.** Fit of the O 1s absorption spectrum with Gaussian functions.

gives us a measure of the O 2p contribution to the vacant orbital, and likewise, the C 1s structure informs on the C 2p content. Second, observation of absorption in the photon energy region used for the cross section measurements can give parallel information on resonance processes that may result in photoionization. An example of this is Re 5p → 5d

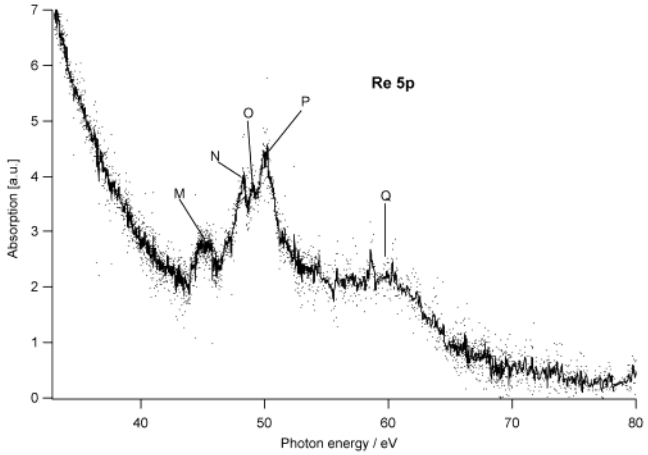


**Figure 12.** Absorption spectra of $ReO_3Me$ in the region 30−80 eV.

**Table 5.** $ReO_3Me$ Absorption Bands, Energies (eV), Relative Intensities, and Assignments, Calculated Energies (eV) and AO Coefficients of Low Lying Vacant Energy Levels of $ReO_3Me$, and Predicted Band Intensities

| band | energy | int | assignment | calcd energy | calcd rel int |
|---|---|---|---|---|---|
| M | 44.9 | | $4a_1 \rightarrow$ Re np | | |
| N | 48.2 | | Re 5p → 6e | 46.1 | 3.1 |
| O | 49.0 | | Re 5p → $6a_1$ | 48.7 | 1.0 |
| P | 50.0 | | Re 5p → 7e | 49.1 | 1.1 |
| Q | 59.7 | | Re 5p $^2P_{1/2}$ | | |
| R | 266.6 | | Re 4d $^2D_{5/2}$ | | |
| S | 279.6 | | Re 4d $^2D_{3/2}$ | | |
| T | 286.1 | | C 1s → $6a_1$ | 285.8 | |
| U | 287.7 | | | | |
| V | 288.8 | | | | |
| X | 530.4 | 4.6 | O1s → 6e | 530.4 | 4.1 |
| Y | 532.8 | 1 | O1s → $6a_1$ | 532.9 | 1.0 |
| Z | 533.6 | 3.1 | O1s → 7e | 533.6 | 3.0 |

excitation followed by super Coster Kronig (SCK) decay resulting in the ionization of 5d electrons.

**O 1s Edge.** Figure 10a shows the absorption spectrum of $ReO_3Me$ in the photon energy region 525−580 eV. The near edge structure shows two strong bands with maxima at 530.4 eV (X) and 533.6 eV (Z). The first band X has an asymmetric shape. The second band has a leading shoulder which deconvolution places at 532.8 eV (Y). These transitions are readily assigned to excitation from O 1s to the 6e, $6a_1$, and 7e orbitals (Table 3). In tetrahedral symmetry, the d orbitals split e < $t_2$. On lowering the symmetry to $C_{3v}$, the $t_2$ level splits into $a_1$ and e levels. In $ReO_3Me$, the covalent nature of the molecule means that the d orbitals are strongly mixed with those of the ligands, and all these levels are expected to have O 2p character. The spacing of the lowest lying empty orbitals ($6a_1$−6e = 1.9 eV; 7e−$6a_1$ = 0.8 eV) is in reasonable agreement with the spacing of the main features of the O 1s absorption spectra (Y−X = 2.4; Z−Y = 0.8 eV). Explicit calculation of the O 1s to 6e, $6a_1$, and 7e excitation energies gave values of 530.4, 532.8, and 533.4 eV in excellent agreement with the experimental data (Table 5). Thus, we can assign the transitions O1s → 6e (X), $6a_1$ (Y), 7e (Z).

The relative intensities of these three transitions were estimated by assuming that only one-center $\langle O(1s)|e\mathbf{z}|O(2p)\rangle$ integrals are significant and two-center contributions to the

transition moment may be neglected. The ground state wave function was used to obtain coefficients of the O(1s) orbitals in the core states and O(2p) orbitals in the three excited states. The calculated relative intensities are given in Table 5. The estimate of 4.1:1.0:3.0 is in good agreement with that obtained from the band areas, i.e., 4.6:1.0:3.1 (Figure 11). The relative areas of bands Y and Z are dependent on the deconvolution of the shoulder, Y. However, the relative areas of X/(Y + Z), on which much more confidence may be placed, is 1.1:1.0 and is close to the estimate of 1.0:1.0. The statistical ratio from orbital degeneracy would be 2:3. Thus, the calculation provides a good model for the AO contributions to the lowest unoccupied orbitals of the molecule.

Band X has an asymmetric profile. One possible cause of this is splitting of the $(O1s)^{-1}(6e)^1$ excited state by either spin−orbit coupling or Jahn−Teller distortion.

**Re 4d Edge.** Figure 10b shows the absorption between 240 and 300 eV. Two broad absorption bands are observed at 266.6 and 270.6 eV, which are assigned to Re 4d excitation. The splitting of the $^2D_{5/2}$ and $^2D_{3/2}$ core holes is 14.0 eV. (The literature value for this splitting is 14 eV.[21])

C 1s excitation also occurs in this spectral range. The C 1s XAS is not well defined, due to the strong photon flux drop as a result of the carbon contamination of the first optical elements of the beamline. Of the three empty valence levels, only the $6a_1$ has a C 2p contribution. Hence, in this case, we only expect one strong band in the near edge structure. Calculation estimates the energy of the C(1s) → $6a_1$ transition as 285.8 eV.

**Absorption Spectrum Between 35 and 80 eV.** The absorption spectrum in this region (Figure 12) shows complex structure between 40 and 70 eV. This range would include any Re 4f and 5p excitations. Excitation of 4f electrons is expected to be of low probability in comparison with 5p. Transitions of 5p → 5d type are favored as they can occur within the same principal quantum shell. We thus expect to access the same 6e, $6a_1$, and 7e orbitals as the O 1s excitations, but in this case by virtue of their Re 5d character.

Bands N, O, and P fit nicely with this hypothesis. Their separations are slightly different from those of bands X, Y, and Z (O−N = 1.8 eV, P−O= 1.0 eV) but still compatible with the orbital splittings calculated for the ground state. So, we assign N, O, and P to the 5p → 6e, $6a_1$, and 7e transitions, respectively. Signal-to-noise on these absorption bands prevents a good fit of the band areas. These features were reproducible over a number of scans on different occasions. The calculated transition energies are given in Table 5, together with the calculated relative intensities of the absorption bands (3.1:1.0:1.1). The appearance of bands N, O, and P is consistent with this.

Band Q, whch is broad and featureless, lies around 11 eV higher than the centroid of N,O, and P; the separation is the size of the spin−orbit splitting of a Re 5p hole. Thus, Q is assigned to Re 5p excitation resulting in a $^2P_{1/2}$ hole state. The absence of structure may be due to the lower inherent intensity of this excitation and the high signal-to-noise levels. However, $^2P_{1/2}$ fine structure is generally observed to be broader than that of $^2P_{3/2}$ as a result of shorter lifetimes.

If the described assignments of N−Q are correct, band M cannot be associated with a primary Re 5p excitation. Its origin will be discussed in the following section in the context of the resonances observed in the cross sections of the valence bands.

**Relationship Between Cross Sections and Absorption Spectra.** Examination of the cross section data derived in preceding sections led to the proposal of possible resonance structures at 35, 38, 43, 47, and 58 eV. The resonances at 47 and 58 eV have energies that coincide with the onset of bands N and Q in the absorption spectra. Bands N−Q have been convincingly assigned to 5p → 5d excitations. Thus, the absorption experiment monitors the initial step in the photoemission resonance, which is ascribed to 5p to 5d excitation followed by SCK decay resulting in the ejection of valence electrons with 5d character. The coincidence of the two features provides confirmation of the assignment of both.

Band D, assigned to the $4a_1$ orbital, has a resonance with an onset energy of 43 eV. There is no analogue in any other band. Band M in the absorption spectrum has a maximum at 45 eV. It seems likely that these two features are related, and that band M results from excitation from the s-like $4a_1$ orbital into a bound level in the continuum of p-like character, in $C_{3v}$ e or $a_1$ symmetry.

**Comparison with $TiCl_3Me$.** In order to facilitate a comparison between $ReO_3Me$ and $TiCl_3Me$, the electronic structure of the latter was calculated with comparable functional and basis sets to those used for $ReO_3Me$. The orbital ordering and composition were similar to those reported previously, but the orbital energies differed somewhat.[4]

The energy level diagrams of $ReO_3Me$ and $TiCl_3Me$ are correlated in Figure 13a. Cartoon representations of the orbitals are given for each energy level. Figure 13b shows the parallel correlation between their PE spectra. Various points are immediately apparent by examination of the figure.

The nonbonding Cl or O based $1a_2$ and 5e orbitals are comparable in energy. Orbitals involving metal d character are stabilized in $ReO_3Me$ compared with $TiCl_3Me$; they have generally higher coefficients for the Re 5d AO than the Ti 3d ones showing greater covalency in the former molecule. The Ti−Me $\sigma$ bond and the C−H bonds are localized in the $5a_1$ and 2e orbitals, respectively. In $ReO_3Me$, these basis orbitals mix with the O 2p orbitals, and ReMe character is distributed throughout the valence orbital manifold.

The overall ordering of the orbitals in $TiCl_3Me$ is (b = bonding, nb = nonbonding)

$$\text{Ti}-\text{C}(\sigma) > \text{Cl}(\pi\ \text{nb}) > \text{Cl}-\text{Ti}(\pi\ \text{b}) > \text{Cl}-\text{Ti}(\sigma\ \text{b}) > \text{C}-\text{H} \quad \text{(b)}$$

Thus, the bond character determines the energy ordering.

For $ReO_3Me$, we find that, as for $OsO_4$, $\sigma-\pi$ mixing is prevalent, orbitals are delocalized over the whole ligand set, and it is the metal orbital character that determines the energy

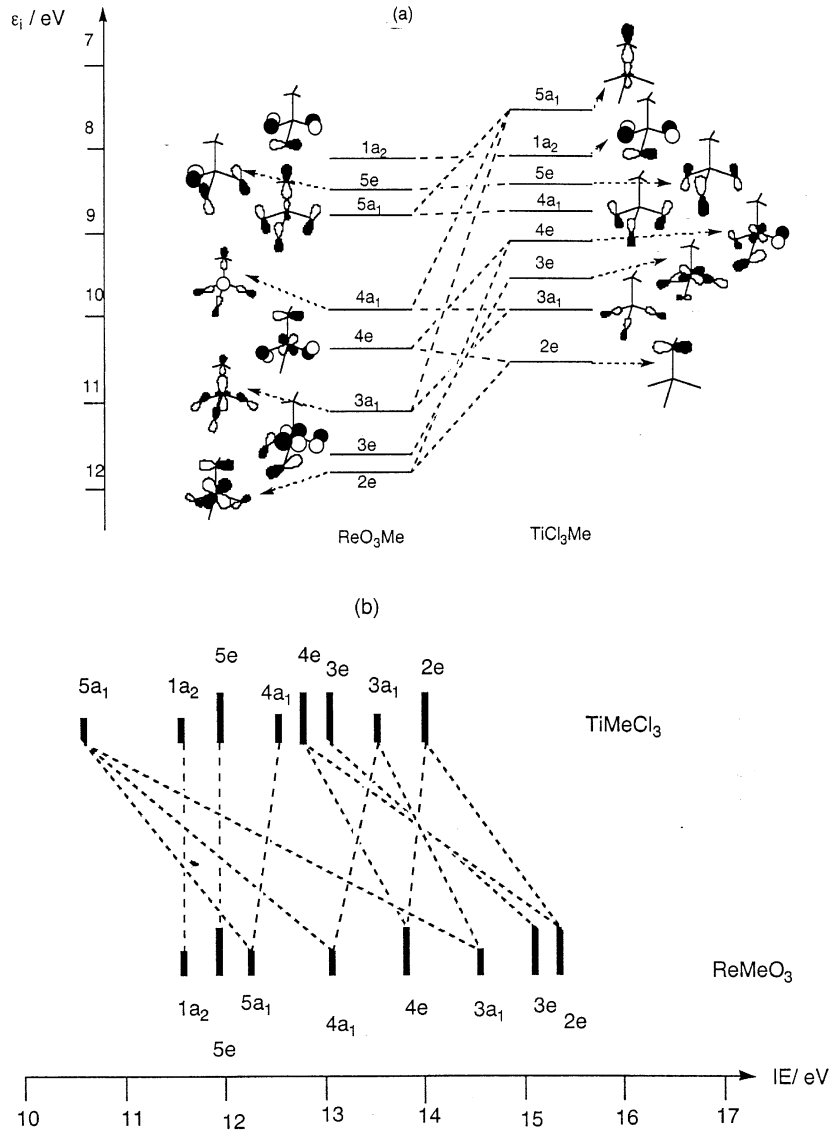


**Figure 13.** Correlation of (a) MO diagrams and (b) PE spectra for $ReO_3Me$ and $TiCl_3Me$.

ordering, i.e.

$$O(nb) > Re(6p) > Re(6s) > Re(5d)$$

While $TiCl_3Me$ and $ReO_3Me$ are geometrically very similar, their electronic structures and chemistries are remarkably different. Thus, while each exhibits pronounced Lewis acidic character associated with a low lying vacant orbital of metal d character, this marks the extent of their similarity.

The most striking difference between $TiCl_3Me$ and $ReO_3Me$ is the nature of the M−C moiety. The HOMO in $TiCl_3Me$ is a localized orbital composed of Ti($d_{z^2}$) and C($p_z$). This, allied to the high polarity of the Ti−C bond, endows it with a high lability. Hence, oxidation proceeds readily by insertion to give $TiCl_3OMe$, protonic species cause the immediate evolution of $CH_4$,[22] and the reagents $HgCl_2$, $SnCl_4$, and $AlCl_3$ each exchange the methyl group to produce $TiCl_4$.[23] Thermal decomposition of $TiCl_3Me$ also appears to proceed through this Achilles' heel, with evolution of $CH_4$ and $CH_3Cl$ and formation of a polymeric material of indeterminate stoichiometry. $TiCl_3Me$ and related TiMe complexes have been long known to have high activity in the Ziegler−Natta catalysis of alkene polymerization,[24] which proceeds by the mechanism whose general features were first proposed by Cossee,[25] involving direct and facile insertion of the alkene $C_2$ unit into the labile Ti−C bond.

In contrast, $ReO_3Me$ is a thermally robust material which is air- and water-stable. Both the Re−C and Re═O moieties are strongly bonded, with Re−X distances corresponding to bond orders greater than 1 and 2, respectively,[6] according with the conclusions of our study which shows the Re−C and Re−O bonding electrons to lie at least 1.5 eV deeper in energy than their counterparts in $TiCl_3Me$ (Figure 13a). In the case of $ReO_3Me$, the frontier orbitals possess mainly Re−O $\pi$-character, with the Re−C bonding electrons distributed between HOMO − 3 and HOMO − 4 and being subject to a significant amount of delocalization over the

(22) Beerman, C.; Bestian, H. *Angew. Chem.* **1959**, *71*, 618.
(23) Ademan, E. H. *J. Polym. Sci., Polym. Symp.* **1968**, *16*, 3643.
(24) Brintzinger, H. H.; Fischer, D.; Mullhaupt, R.; Rieger, B.; Waymouth, R. *Angew. Chem., Int. Ed. Engl.* **1995**, *34*, 143.
(25) Arlman, E. J.; Cossee, P. *J. Catal.* **1964**, *3*, 99.

metal and the oxygen ligands. The Re−C bond thus plays a less prominent role in the chemistry of the compound than does its counterpart in $TiCl_3Me$. Rather, is it the Re−O moieties which characterize the majority of the chemistry displayed. $ReO_3Me$ is a highly versatile oxidizing agent in organic chemistry,[5] with alkene epoxidation, Baeyer−Villiger reactions, and aromatic oxidation being readily effected through intermediate peroxo derivatives which permit oxidation to proceed while preserving the parent Re−O moieties.[26,27] However, the Re−C bond does play an pivotal role in alkene metathesis, for which $ReO_3Me$ and related Re(VII) species have been shown to have high activity.[28,29] This reaction is generally considered to proceed by the mechanism proposed by Chauvin, involving the intermediacy of alkylidene complexes, with the Re═C moiety being regenerated in the catalytic cycle.[30,31] Hence, rather than M−C bond fission, it is the formation of a rhenium−carbon double bond which facilitates alkene metathesis. Indeed, matrix-isolated $ReO_3Me$ has been shown to tautomerize to such a methylidene species under the influence of UV light.[17,32] Hence, the strength, stability, and covalent nature of the Re−C bond in $ReO_3Me$ endow it with a chemistry markedly different from that displayed by its counterpart in $TiCl_3Me$.

(26) Al-Ajlouni, A. M.; Espenson, J. H. *J. Org. Chem.* **1996**, *61*, 3969.
(27) Abu-Omar, M. M.; Espenson, J. H. *Organometallics* **1996**, *15*, 3543.
(28) O'Connor, J. M. In *Comprehensive Organometallic Chemistry II*; Casey, C. P., Ed.; Pergamon: Oxford, U.K., 1995; Vol. 6, p 200.
(29) Hoffmann, D. M. In *Comprehensive Organometallic Chemistry II*; Casey, C. P., Ed.; Pergamon: Oxford, U.K., 1995; Vol. 6, p 231.
(30) Herrisson, J. L.; Chauvin, Y. *Makromol. Chem.* **1970**, *141*, 161.
(31) Casey, C. P.; Burkhardt, T. P. *J. Am. Chem. Soc.* **1974**, *96*, 7808.
(32) Morris, L. J.; Downs, A. J.; Greene, T. M.; McGrady, G. S.; Herrmann, W. A.; Sirsch, P.; Gropen, O. *Chem. Commun.* **2000**, 67.

## Conclusions

PE cross sections of the valence region of $ReO_3Me$ confirm a computational model of the molecule. The electronic structure is most readily described as a perturbed tetrahedral $d^0$ system with the most strongly bound orbitals being those with significant 5d character. Absorption spectra provide evidence for the resonant processes observed in the photoionization cross sections. They also indicate strong Re 5d O 2p mixing in the lowest unoccupied orbitals.

In contrast to a previous study on $TiCl_3Me$, where the methyl ionizations were associated with two spectral bands, both the C−H bonds and the Re−C bonds in $ReO_3Me$ contribute to several MOs. The contrasting nature of the chemistry of the two systems may be accounted for by these differences in electronic structure.

**Acknowledgment.** We thank the EU for financial support which enabled the use of the ELETTRA synchrotron at Trieste. Part of this work has been carried out using the computational resources of a DEC8400 multiprocessor cluster (Columbus/Magellan), provided by the U.K. Computational Chemistry Facility at Rutherford Appleton Laboratory, and part using the facilities of the Oxford Supercomputing Centre.

IC020547+